

Metrology requirements for the integrated luminosity measurement using small-angle Bhabha scattering at ILC

Ivan Smiljanić¹, Ivanka Božović¹, Goran Kačarević¹, Mirko Radulović², and Jasna Stevanović²

¹*Vinca Institute of Nuclear Sciences - National Institute of the Republic of Serbia, University of Belgrade, M. Petrovica Alasa 12-14, Belgrade, Serbia*

**E-mail: i.smiljanic@vin.bg.ac.rs*

²*University of Kragujevac, Faculty of Science, 34000 Kragujevac, Serbia*

.....
Precision measurement of the integrated luminosity \mathcal{L} at future Higgs factories, including ILC, is of crucial importance for the cross-section measurements, and in particular for the line-shape measurements at the Z-pole. Since there is no up-to-date estimate of the integrated luminosity uncertainties arising from metrology effects at ILC, here we review the metrology requirements for the targeted precision of \mathcal{L} at foreseen ILC center-of-mass energies: 91.2 GeV, 250 GeV, 500 GeV and 1 TeV, using small-angle Bhabha scattering.

arXiv:2407.03024v3 [hep-ex] 28 Oct 2024

1 Introduction

The realistic target for integrated luminosity (\mathcal{L}) precision at future high energy electron-positron colliders is set by the requirements of their physics programs, primarily aiming to study the properties of a Higgs boson in the operation mode at around 250 GeV center-of-mass energy. For the most of these measurements, relative systematic uncertainty of the integrated luminosity of $\sim 10^{-3}$ should suffice. The same holds for a TeV scale directly accessible at linear colliders like ILC [1]. At lower center-of-mass energies dedicated for precision EW studies, the targeted luminosity precision is set to $\sim 10^{-4}$, primarily from the line-shape measurements at the Z resonance and the W boson mass measurement from the W-pair production line shape at the threshold [2].

The feasibility of such required precision is challenged by numerous requirements related to manufacturing, positioning and performance of the luminosity monitor, in addition to the uncertainties of beam properties (transverse and longitudinal sizes, energy and beam delivery to the interaction point), collectively referred to as metrology. These effects impact the available phase space for detection of the final state particles and consequently their count, introducing systematic uncertainty in the integrated luminosity measurement.

Since the monitoring systems for most of these effects are under development at ILC, this paper aims to provide tolerable margins for the effects under study from the point of view of the integrated luminosity precision goals. Each effect is set to contribute to the relative uncertainty of the integrated luminosity as $1 \cdot 10^{-3}$ ($1 \cdot 10^{-4}$) at the center-of-mass energy of 250 GeV and above (at the Z-pole), limiting the overall contribution from metrology to the relative uncertainty of \mathcal{L} to less than $3.3 \cdot 10^{-3}$ ($3.3 \cdot 10^{-4}$), since many of the precision margins presented here can be easily surpassed with the existing technologies. As pointed out in the Focus topics document for the ECFA study on Higgs/top/EW factories [3], the impact of metrology on the integrated luminosity measurement at ILC has not been estimated yet, up to the generic study for a long time ago proposed TESLA collider [4] discussed in [5].

This study is based on the small angle Bhabha scattering (SABS), the conventionally used process as a large rate, almost pure QED process with the theoretical uncertainty of $3.7 \cdot 10^{-4}$ recently revised for the LEP analyses [6], although neither NLO electroweak corrections nor the multi-fermion production are implemented in the existing Bhabha MC tools [3]. Once the SABS cross-section (σ) is known in a certain phase space, the number of Bhabha counts (N) can be used to measure the integrated luminosity as $\mathcal{L} = \frac{N}{\sigma}$. The uncertainty of Bhabha's count is translated as the uncertainty of \mathcal{L} .

The structure of the paper is the following: Section 2 brings a brief overview of instrumentation of the very forward region at ILC and the considered systematic effects, while

Section 3 brings limits on the detector and beam-related parameters at center-of-mass energies foreseen at ILC, assuming the maximal contribution per effect of 10^{-3} (10^{-4}) at the center-of-mass energy of 250 GeV and above (at the Z-pole).

2 Luminosity measurement at ILC

There was an extensive work by the FCAL Collaboration on luminometer design, performance and prototyping, documented in [7], [8] and [9]. The FCAL Collaboration has proposed instrumentation of the very forward region of the ILD detector at ILC [10] with two SiW sandwich calorimeters, one for the fast luminosity estimate and measurement of the beam properties (Beam Cal) and the other for measurement of the integrated luminosity (LumiCal). The feasibility of realization of these devices has been proven in several test beam campaigns, demonstrating performance of a calorimeter prototype [7]. Systematic uncertainties from the luminometer performance are discussed in [8], while the impact of beam related effects on reconstruction of the luminosity spectrum is discussed in [9]. As pointed out, systematic effects from metrology have not been quantified yet.

2.1 Instrumentation of the very forward region

The layout of the very forward region at ILD is given in Figure 1 [8]. At 2500 mm from the IP, a luminometer will be centered around the outgoing beam at 7 mrad polar angle with respect to the z-axis, preserving the symmetry of head-on collisions at ILC with the crossing angle of 14 mrad. The geometrical aperture of the luminometer is 31-77 mrad, while the sampling term is constant in the range of 41-67 mrad, which defines the fiducial volume (FV) [8]. The luminometer consists of 30 subsequent Si-W layers providing longitudinal coverage for showers developed from high-energy Bhabhas. Each layer (including the Si sensor, capton HV and fan-out, together with the supportive structure) is 640 μm thick. To provide precision position measurement in the transverse plane, Si sensors are finely segmented into pads (48 azimuthal sectors and 64 radial rings), each with 1.8 mm pitch.

The study presented in this paper relies only on the size of the fiducial volume and its effective change due to the effects to be described (Section 2.3) without taking into consideration detector performance based on the given choice of technology.

2.2 Event generation

We have simulated 10 million small angle Bhabha scattering events using the BHLUMI V4.04 Bhabha event generator [11] for each energy considered. Bhabha events are generated

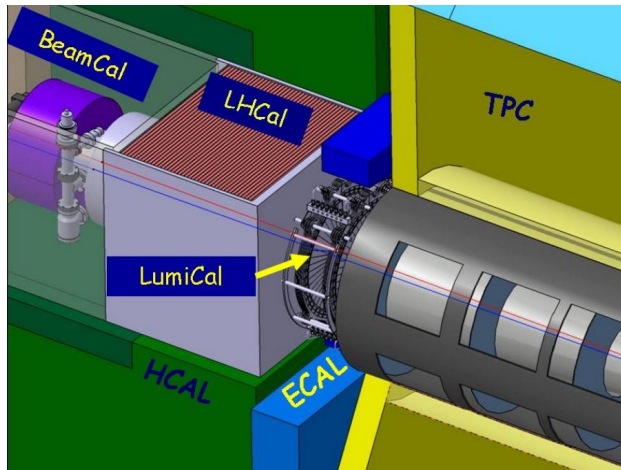


Fig. 1: Layout of the very forward region of a detector at ILC, with luminometer placed 2500 mm from the IP.

from 20 mrad to 200 mrad, to allow events with non-collinear final state radiation to contribute. Initial state radiation is also considered while beam-beam interactions are neglected. Also, we do not consider electromagnetic deflection of the final state due to interactions with the field of the corresponding outgoing beam. These effects have been discussed in [9]. Also, in [9] it has been shown that the luminometer at ILC will not be significantly affected by the four-fermion background from the Landau-Lifshitz type of processes (‘two-photon’ exchange), so we do not consider it here either. Bhabha cross-sections in the considered range of polar angles are: 161.5 nb, 22.4 nb, 4.5 nb and 0.79 nb, at the Z-pole, 250 GeV, 500 GeV and 1 TeV center-of-mass energy, respectively. Expected integrated luminosities assume the so called H-20 staged run [12] of ILC at 250 GeV and 500 GeV with the corresponding integrated luminosities of 2 ab^{-1} and 4 ab^{-1} , to be complemented with 8 ab^{-1} of data at 1 TeV center-of-mass energy and 100 fb^{-1} at the Z-pole. Figure 2 [13] illustrates estimated ILC running time and integrated luminosities in the H-20 operating scenario.

We have applied asymmetrical event selection in polar angles (AS1), in a way that at one side of the luminometer a full fiducial volume is considered, while at the other side the inner and outer radii of the fiducial volume are narrowed by 1 mm. Modification of the counting volume is applied subsequently on the left and right arm of the luminometer, on event-by-event basis. This approach (with some variations between experiments) has been applied at LEP [14], reducing the net systematic effect arising from left-right asymmetries. This, however, requires that the luminometer arms are positioned on the outgoing beams at colliders with a non-zero crossing angle. It should be noted that the statistical fluctuation

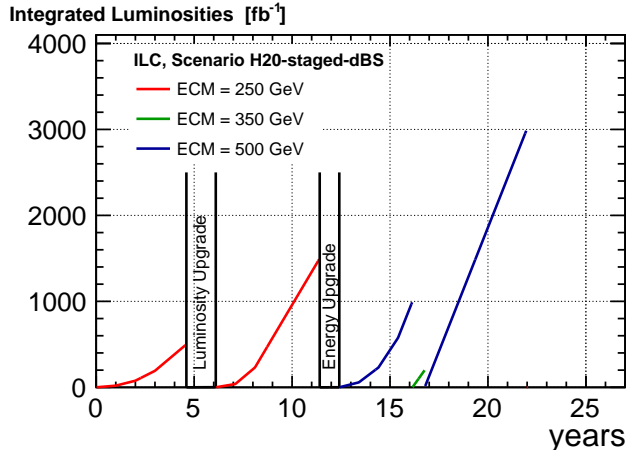


Fig. 2: Integrated luminosity vs. ILC running time in the H-20 operating scenario.

of generated samples is of order of $3 \cdot 10^{-4}$ and for this reason we rather illustrate the dependences of the effects under study then attempting to model an effect with a fit.

2.3 Effects from metrology

We are considering the following systematic effects that will be present due to the uncertainties of the luminometer radial dimensions, positioning with respect to the IP and relative positioning of detector halves, as well as due to luminometer vibrations in the transverse and longitudinal direction:

- (1) uncertainty of the inner radius of the luminometer's counting volume (Δr_{in}),
- (2) uncertainty of the outer radius of the luminometer's counting volume (Δr_{out}),
- (3) RMS of the Gaussian spread of the measured radial shower position with respect to the true hit position¹ (σ_r),
- (4) uncertainty of the longitudinal distance between left and right halves of the luminometer (Δl) assuming that both halves are moving simultaneously towards the IP or away from it for $\Delta l/2$,
- (5) RMS of the Gaussian distribution of mechanical fluctuations of the luminometer with respect to the IP in the radial direction ($\sigma_{x_{IP}}$),
- (6) RMS of the Gaussian distribution of mechanical fluctuations of the luminometer with respect to the IP in the axial direction ($\sigma_{z_{IP}}$),

¹ True Bhabha position can be measured by placing a Si tracker plane in front of the luminometer with the precision of several microns. In addition, this would provide electron-photon separation.

- (7) tilt of the luminometer (both arms) equivalent to a rotation around y-axis for a certain angle (tilt).

Also, the beam bunches are finite in size and interaction may occur anywhere inside the bunches. In addition, beam synchronization may cause longitudinal (axial) displacements of the IP. Thus we consider:

- (8) radial (Δx_{IP}) displacements of the interaction point with respect to the luminometer,
- (9) axial (Δz_{IP}) displacements of the interaction point with respect to the luminometer. From Δz_{IP} , maximal time shift in beam synchronization ($\Delta\tau$) can be determined.

Any asymmetry of the beam energies occurring either on an event-by-event basis as a random variation due to the beam energy spread (BES) or as a permanent bias of one beam energy with respect to the other, will cause a boost (assumed longitudinal²) of the initial and consequently of the final electron-positron system. The boost (β_z) of Bhabha particles will lead to an effective change of the luminometer acceptance seen from the final state electron (positron) reference frame and to the consequent change of the Bhabha count. We thus consider two additional systematic effects:

- (10) RMS of the Gaussian distribution of the beam energy spread ($\sigma_{E_{BS}}$) and
- (11) difference in energy (ΔE) between the colliding beams.

Every effect is individually considered to lead to the overall relative change of count of 10^{-4} (10^{-3}) at the Z-pole (higher center-of-mass energies). In this respect, the maximal tolerance is derived for the parameters under study.

3 Precision requirements for the integrated luminosity measurement

Precision requirements for the integrated luminosity measurement translates to a similar precision requirements on the center-of-mass energy, since the Bhabha cross-section scales with the center-of-mass energy as $\propto 1/s$. In the range of the ILC energies, the center-of-mass energy should be known at the level of several MeV at the Z-pole, to a few hundred MeV at higher center-of-mass energies. The latter seems to be feasible with experimental reconstruction of di-muon processes at 250 GeV center-of-mass energy [15], providing \sqrt{s}

² For the boost to be longitudinal, we assume that the initial state radiation is emitted along the z-axis (in the head-on collisions) and that the final state radiation is emitted in the direction of a final state electron (positron).

absolute precision of the order of the beam energy spread of 0.19% [16]. At the Z-pole, the situation seems to be more challenging. However, for the cross-section measurements of the s-channel processes with the similar cross-section dependence on s , uncertainties arising from the limited knowledge of the center-of-mass energy will cancel out in the luminosity estimate.

A whole set of effects will stem from the detector capability to measure energy and position of scattered Bhabha electrons (positrons). We do not discuss these effects further, since the performance of the luminometer in terms of energy and position reconstruction is not yet fully known. In [7] it is demonstrated that the prototype of the luminometer with six detector planes can reconstruct the signal hits with the resolution of $440 \mu\text{m}$ in the front plane. In this section we shall consider the required resolution at various ILC center-of-mass energies.

3.1 Z-pole

Figures 3 (a) to 13 (a) illustrate the dependence of the relative change of Bhabha count ($\Delta N/N$) on the metrology effects listed as 1 to 11 respectively. As the maximal value for each effect we take the one corresponding to $\Delta\mathcal{L}/\mathcal{L} = \Delta N/N = 10^{-4}$. If there is more than one value of the metrological uncertainty corresponding to this luminosity (count) precision, the smaller tolerance is taken (i.e. $\Delta r_{in}, \Delta l, \Delta x_{IP}, \Delta z_{IP}$). All the fluctuations that can be seen on Figures 3 to 13 for all energies are of statistical nature, caused by the limited size of samples.

As can be seen from Figures 3 (a) to 13 (a), the most challenging requirement at the Z-pole comes from the precision of the inner radius of the counting volume of a luminometer. If events are counted in a symmetrical way considering the full detector acceptance on both sides, a precision of the inner aperture of the counting volume of $\sim 3 \mu\text{m}$ is required. However, the asymmetrical counting with sufficiently large reduction of the inner radius of the counting volume at one side of the detector (i. e. $\Delta r = 1 \text{ mm}$) compensates for the counting loss at the other side caused by the (smaller) variations of the counting volume, thus relaxing the maximal uncertainty of the inner radius of the counting volume to $\sim 20 \mu\text{m}$ (Figure 3 (a)). A full simulation of the luminometer response to showers produced by SABS is needed to understand how the uncertainty of the inner aperture of the device transfers to the fiducial volume as the counting region.

Other metrology effects related to luminometer positioning are ranging from a few hundreds of micrometers to several millimeters; these should not be an issue for contemporary laser positioning systems based on frequency scanning interferometry. In a system implemented in the ATLAS experiment, $1 \mu\text{m}$ absolute precision in positioning can be reached over 1 m distance [17]. The luminometer should be aligned with the outgoing beam with a tilt

no larger than ~ 14 mrad (Figure 9 (a)). A dedicated luminometer positioning system would have to be developed to ensure the feasibility of this precision. If the axial displacement of the IP was caused by beam synchronization (Figure 11 (a)), the time shift between beams should not be larger than ~ 13 ps. Beam spread at the Z-pole should not be larger than ~ 110 MeV (Figure 12 (a)), what can be accomplished assuming that the BES is not larger than 0.25%. Eventual difference in energy of one beam with respect to the other should not exceed ~ 5 MeV, the value of the permanent bias which is highly unlikely to occur.

3.2 Higher center-of-mass energies

Similarly to the Z-pole, Figures 3 (b) to 13 (b) illustrate the dependences of the relative change of Bhabha count ($\Delta N/N$) on the metrology effects listed as 1 to 11 respectively. All three center-of-mass energies share the same precision requirement on the relative systematic uncertainty of the integrated luminosity of 10^{-3} . Dependences and limits on mechanical and beam parameters are similar at the considered center-of-mass energies, so they are collectively given at the same figure per each effect. The size of the uncertainties are given in regions of interest for the targeted precision of $\delta\mathcal{L}$ of 10^{-3} for each individual effect. Also, one should assume that the SABS as a calibration process does not receive any new physics contribution at high center-of-mass energies.

As can be seen from Figures 3 (b) to 13 (b), precision requirements for metrology are typically relaxed a few times and up to an order of magnitude with respect to the ones at the Z-pole. The tilt of the luminometer is tolerable below ~ 35 mrad (Figure 9 (b)) which should be a feasible precision of the angular position control with the laser interferometry based systems. Yet, ILC, as well as the other future Higgs factories, requires a detailed study of a customized solution for position monitoring of subdetectors in the very forward region. An interesting question to be addressed in addition is what will be the impact of the push-pull option [18] on the precision estimates presented in this paper.

The beam related requirements allow IP axial displacements up to 9 mm corresponding to a ~ 30 ps time-shift in beam synchronization, while radial displacements of the IP can be tolerated up to ~ 600 μm which is a very large tolerance with respect to the vertical size of the ILC nano-beams of 5.9 nm (at 250 GeV) [18]. The beam energy spread smaller than 500 MeV (at 250 GeV ILC) will not affect the integrated luminosity measurement in a relevant way, and this margin is two times larger than the beam spread in the current ILC design of $\sim 0.19\%$ [18]. The same holds for higher center-of-mass energies. If an eventual difference of one beam energy with respect to the other would be present, it should not be larger than 1 permille of the beam-energy (Figure 13 (b)) which also seems to be realistic.

Table 1: Maximal absolute precision of luminometer mechanical parameters and beam parameters, each contributing as $10^{-4}(10^{-3})$ to the relative uncertainty of \mathcal{L} at the Z^0 pole (higher energies). Values are approximated from Figures 3 to 13.

parameter	Z-pole	250 GeV	500 GeV	1 TeV
Δr_{in} (μm)	20	200	200	200
Δr_{out} (μm)	60	600	600	550
σ_r (mm)	0.3	0.5	0.5	0.5
Δl (mm)	0.2	2.5	2.5	2.5
$\sigma_{x_{IP}}$ (mm)	0.3	0.6	0.6	0.6
$\sigma_{z_{IP}}$ (mm)	5	10	10	10
$\Delta\varphi$ (mrad)	14	35	35	35
Δx_{IP} (mm)	0.3	0.6	0.6	0.6
Δz_{IP} (mm)	4	8	8	8
$\Delta\tau$ (ps)	13	27	27	30
$\sigma_{E_{BS}}$ (MeV)	110	500	1000	2000
ΔE (MeV)	5	125	250	500

The approximate maximal tolerance of the metrology parameters under study, extracted from Figures 3 to 13 is listed in Table 1.

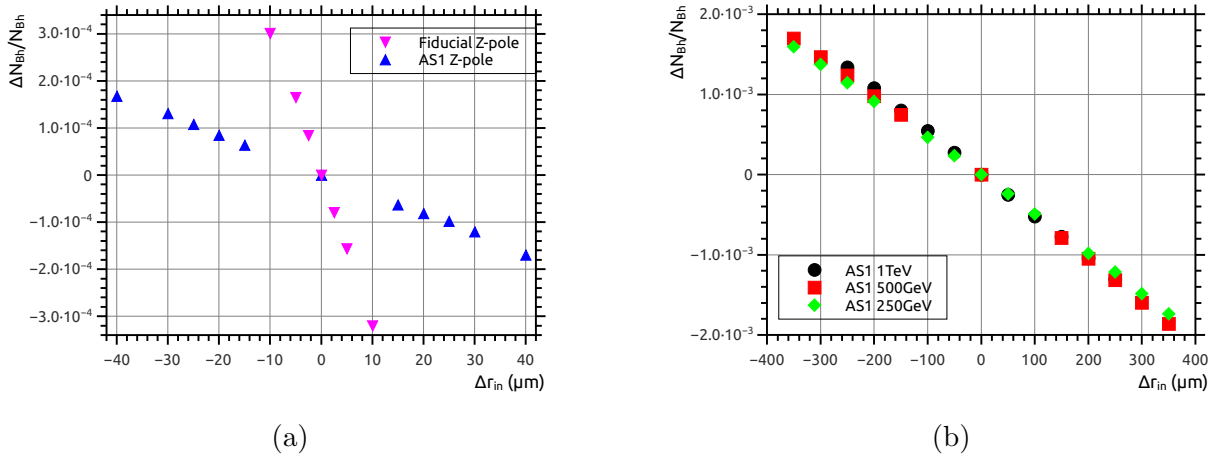
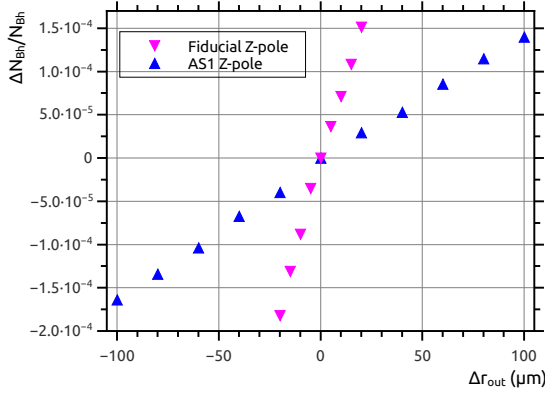
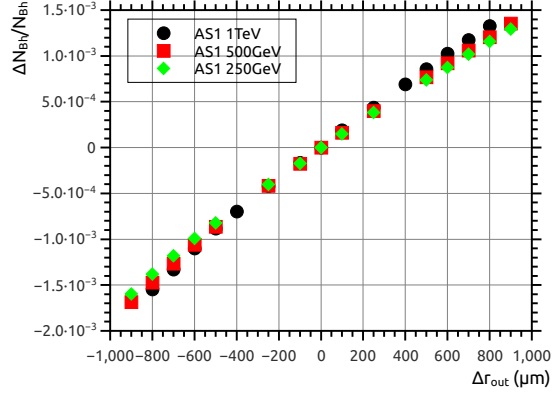


Fig. 3: (a) Impact of uncertainty Δr_{in} of the luminometer FV inner radius on Bhabha counting, at the Z-pole; (b) The same at 250 GeV, 500 GeV and 1 TeV center-of-mass energies for AS1 event selection (Section 2.2).

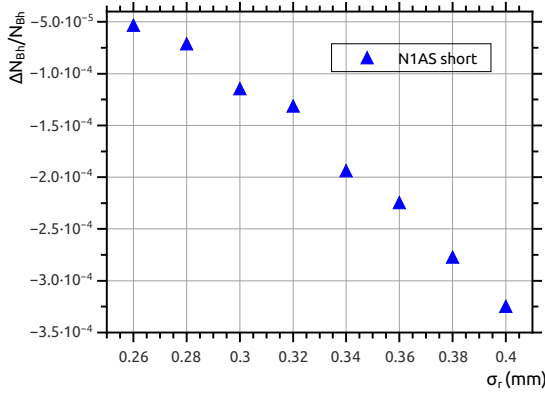


(a)

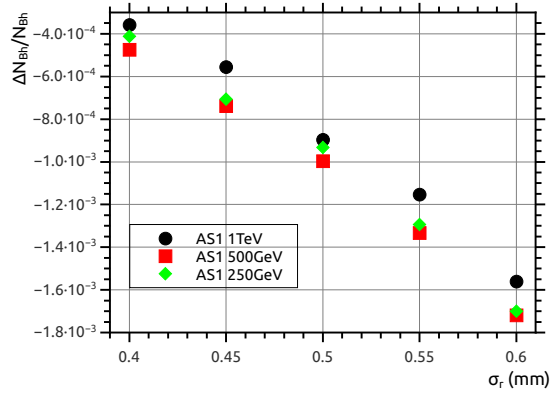


(b)

Fig. 4: (a) Impact of uncertainty Δr_{out} of the luminometer FV outer radius on Bhabha counting, at the Z-pole; (b) The same at 250 GeV, 500 GeV and 1 TeV center-of-mass energies for AS1 event selection (Section 2.2).

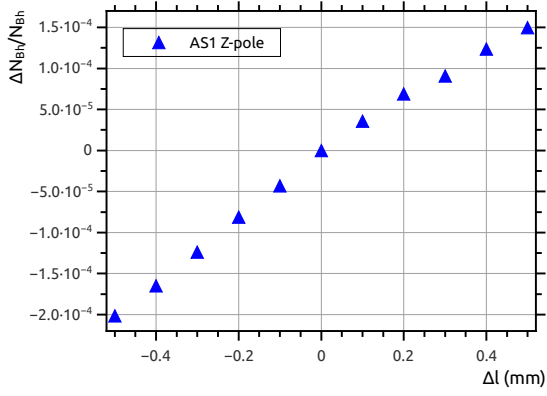


(a)

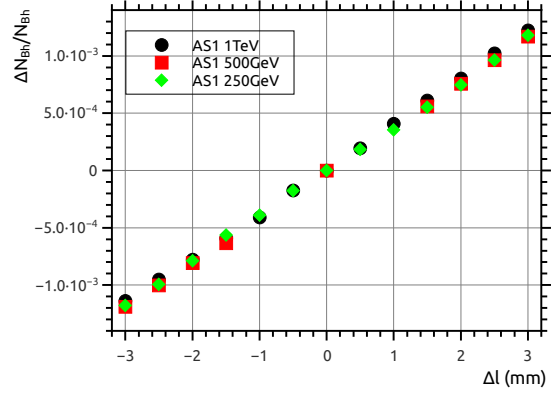


(b)

Fig. 5: (a) Impact of the uncertainty σ_r of measured shower radial position with respect to the true Bhabha position, at the Z-pole; (b) The same at 250 GeV, 500 GeV and 1 TeV center-of-mass energies for AS1 event selection (Section 2.2).

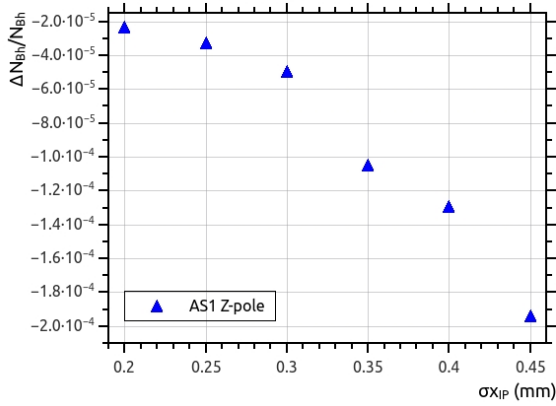


(a)

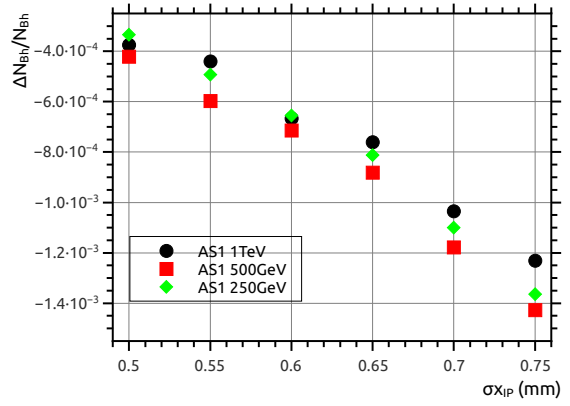


(b)

Fig. 6: (a) Impact of uncertainty of the longitudinal distance Δl between left and right halves of the luminometer, at the Z-pole; (b) The same at 250 GeV, 500 GeV and 1 TeV center-of-mass energies for AS1 event selection (Section 2.2).

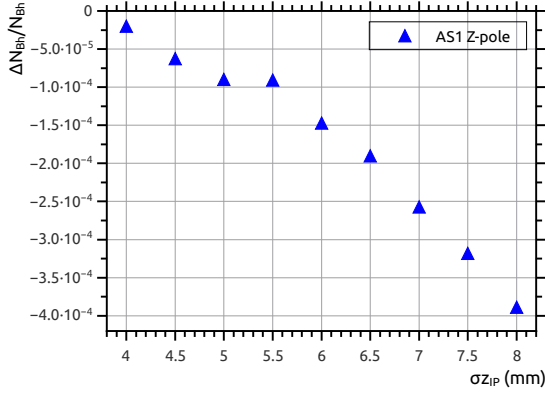


(a)

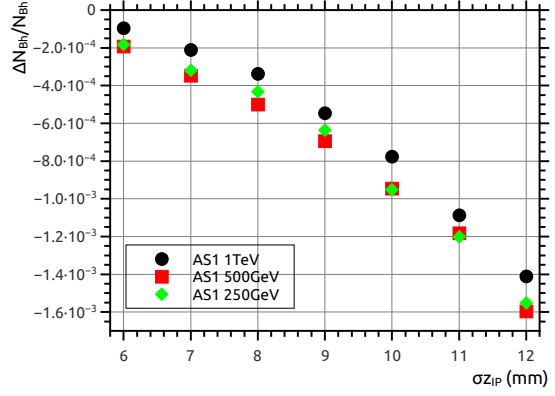


(b)

Fig. 7: (a) Impact of radial fluctuations $\sigma_{x_{IP}}$ of the luminometer with respect to the IP, at the Z-pole; (b) The same at 250 GeV, 500 GeV and 1 TeV center-of-mass energies for AS1 event selection (Section 2.2).

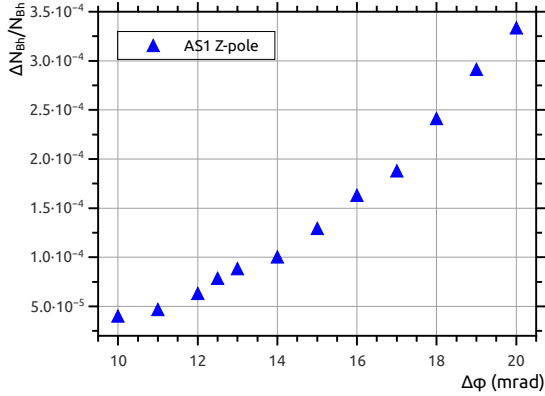


(a)

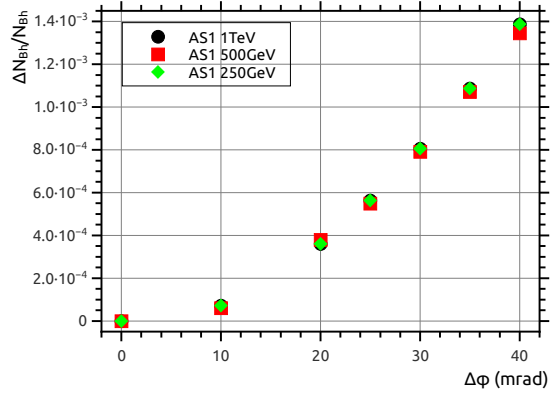


(b)

Fig. 8: (a) Impact of axial fluctuations $\sigma_{z_{IP}}$ of the luminometer with respect to the IP, at the Z-pole; (b) The same at 250 GeV, 500 GeV and 1 TeV center-of-mass energies for AS1 event selection (Section 2.2).

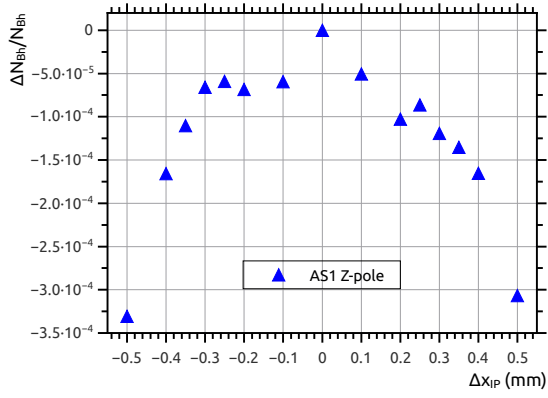


(a)

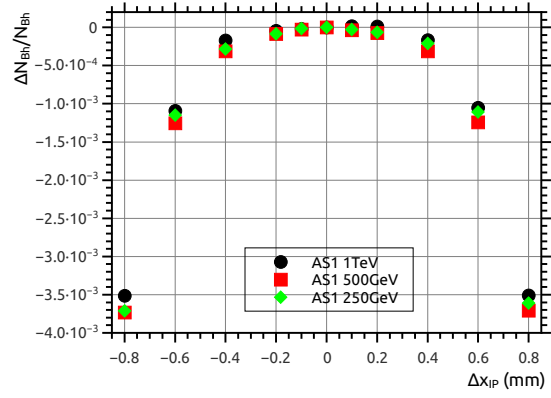


(b)

Fig. 9: (a) Impact of rotation of the luminometer arms around the y-axis for a certain angle $\Delta\phi$ (tilt), at the Z-pole; (b) The same at 250 GeV, 500 GeV and 1 TeV center-of-mass energies for AS1 event selection (Section 2.2).

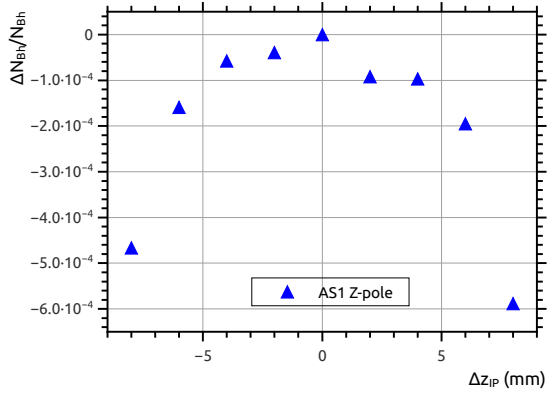


(a)

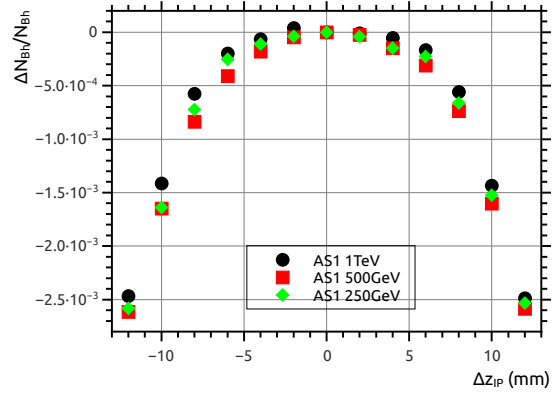


(b)

Fig. 10: (a) Impact of radial displacements Δx_{IP} of the interaction point with respect to the luminometer, at the Z-pole; (b) The same at 250 GeV, 500 GeV and 1 TeV center-of-mass energies for AS1 event selection (Section 2.2).

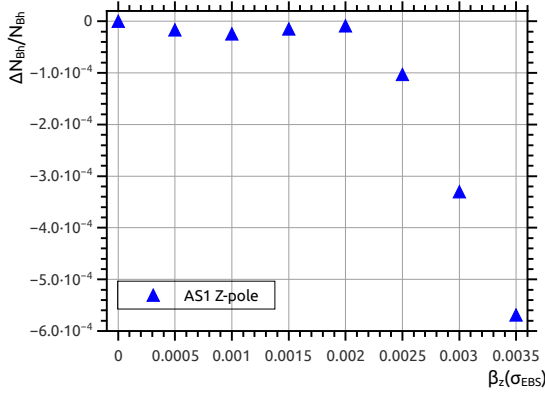


(a)

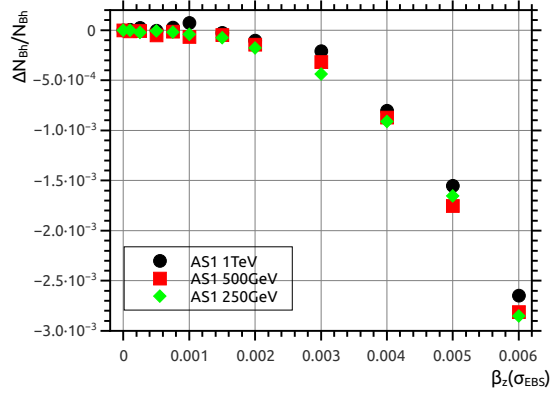


(b)

Fig. 11: (a) Impact of axial displacements Δz_{IP} of the interaction point with respect to the luminometer, at the Z-pole; (b) The same at 250 GeV, 500 GeV and 1 TeV center-of-mass energies for AS1 event selection (Section 2.2).

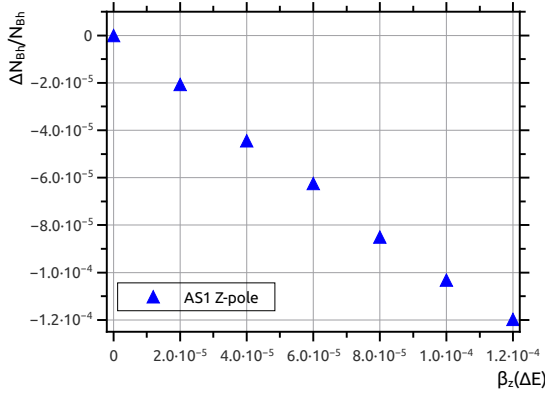


(a)

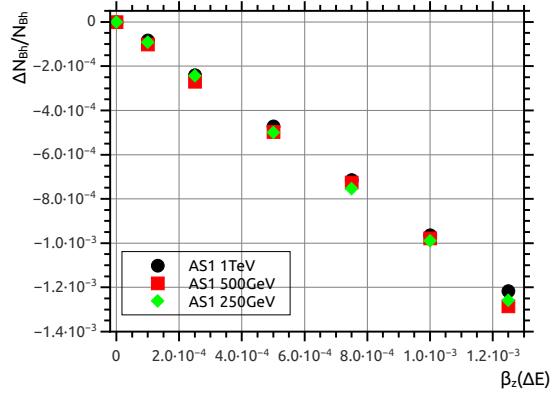


(b)

Fig. 12: (a) Impact of the half-width σ_{EBS} of the Gaussian beam energy spread at the Z-pole as a source of longitudinal boost β_z of the final state; (b) The same at 250 GeV, 500 GeV and 1 TeV center-of-mass energies for AS1 event selection (Section 2.2).



(a)



(b)

Fig. 13: (a) Impact of the difference in energy ΔE between the colliding beams at the Z-pole, producing the longitudinal boost β_z ; (b) The same at 250 GeV, 500 GeV and 1 TeV center-of-mass energies for AS1 event selection (Section 2.2).

4 Conclusion

This paper presents the first review of metrology effects in integrated luminosity measurements at ILC. We consider ILC operating energies at the Z-pole, 250 GeV, 500 GeV and 1 TeV center-of-mass energy. Each individual effect is assumed to contribute to the relative uncertainty of the integrated luminosity at the level of 10^{-4} and 10^{-3} at the Z-pole and higher energies, respectively, so the overall relative systematic uncertainty from metrology is limited to $3.3 \cdot 10^{-4}$ and $3.3 \cdot 10^{-3}$ in the worst case scenario. Since the precision achievable with the existing technologies, and in particular those related to the positioning and the alignment of the luminometer will be much higher than established here, realistic precision of \mathcal{L} from metrology at ILC should be between $1 \cdot 10^{-4}(10^{-3})$ and $3 \cdot 10^{-4}(10^{-3})$ at the Z-pole and higher energies respectively.

This paper quantifies the metrology requirements to achieve the targeted precision and provide the guideline margins for the monitoring systems under development at ILC. At the Z-pole a few challenges are identified, such as the available center-of-mass energy and eventual difference in energy between beams present in a form of bias should be known at the level of ~ 5 MeV. Uncertainty of the luminometer inner aperture is known to be critical due to the $1/\theta^3$ dependence of the Bhabha cross-section on the polar angle. Asymmetric counting with the luminometer positioned at the outgoing beams relaxes to some extent the uncertainty of the inner radius of the counting volume to the level of $\sim 20 \mu\text{m}$. It is yet to be confirmed in a full detector simulation how the uncertainty of the luminometer's inner aperture translates to the definition of the fiducial volume. At studied center-of-mass energies of 250 MeV and above we do not identify critical aspects of metrology from the point of view of existing technologies.

Acknowledgment

This research was funded by the Ministry of Education, Science and Technological Development of the Republic of Serbia and by the Science Fund of the Republic of Serbia through the Grant No. 7699827, IDEJE HIGHTONE-P. The study is done within the framework of ILD Concept Group. The authors would like to thank to the ILD Publication and Speakers Bureau and professor Graham W. Wilson from the Department of Physics and Astronomy, University of Kansas, for very useful comments and suggestions regarding this paper.

References

- [1] The International Linear Collider, Technical Design Report Volume 3. II: Accelerator Baseline Design (2013) [arXiv: arXiv:1306.6328 [physics.acc-ph]]. <https://doi.org/10.48550/arXiv.1306.6328>
- [2] P. Azzurri et al., *Physics Behind Precision* (2017). <https://doi.org/10.48550/arXiv.1703.01626>

- [3] J. de Blas et al. *Focus topics for the ECFA study on Higgs / Top / EW factories*, (2024) [arXiv:2401.07564 [hep-ph]]. <https://doi.org/10.48550/arXiv.2401.07564>
- [4] R.-D. Heuer, *TESLA Technical Design Report Part III: Physics at an e^+e^- Linear Collider* (2001) <https://doi.org/10.48550/arXiv.hep-ph/0106315>
- [5] A. Stahl, LC-DET-2005-004 (2005). <https://bib-pubdb1.desy.de/record/587787/files/LC-DET-2005-004.pdf>
- [6] Patrick Janot, Stanisław Jadach, *Improved Bhabha cross section at LEP and the number of light neutrino species*, *Physics Letters B* 803 (2020) 135319. <https://doi.org/10.1016/j.physletb.2020.135319>
- [7] H. Abramowicz et al. [FCAL Collaboration], *Eur. Phys. J. C* **79**: 579 (2019). <https://doi.org/10.1140/epjc/s10052-019-7077-9>
- [8] H Abramowicz et al. [FCAL Collaboration], *JINST* **5** P12002 (2010). 10.1088/1748-0221/5/12/P12002
- [9] I. Božović Jelisavčić et al., *JINST* **8** P08012 P08012 (2013). 10.1088/1748-0221/8/08/P08012
- [10] ILD Concept Group, *The International Large Detector, Letter of Intent*, DESY 2009-87 (2010). <https://doi.org/10.48550/arXiv.1006.3396>
- [11] S. Jadach et al., *Comput.Phys.Commun.* 102, 229–251 (1997). [https://doi.org/10.1016/S0010-4655\(96\)00156-7](https://doi.org/10.1016/S0010-4655(96)00156-7)
- [12] T. Barklow et al., *ILC Operating Scenarios*, ILC-NOTE-2015-068, arXiv:1506.07830v1 [hep-ex] (2015). <https://doi.org/10.48550/arXiv.1506.07830>
- [13] K. Fujii et al., *Physics Case for the 250 GeV Stage of the International Linear Collider* (2018) [arXiv:1710.07621 [hep-ex]]. <https://doi.org/10.48550/arXiv.1710.07621>
- [14] B. Pietrzyk, LAPP-EXP-94.18 (1994). https://inis.iaea.org/collection/NCLCollectionStore/_Public/26/072/26072195.pdf
- [15] B. Madison and G. W. Wilson, *Center-of-mass energy determination using $e^+e^- \rightarrow \mu^+\mu^-(\gamma)$ events at future e^+e^- colliders* (2022), [arXiv:2209.03281 [hep-ex]],
G. W. Wilson, *Further investigation of dilepton-based center-of-mass energy measurements at e^+e^- colliders* (2023), [arXiv:2308.10414 2209.03281[hep-ex]].
- [16] C. Adolphsen et al., *The International Linear Collider Technical Design Report - Volume 3.I: Accelerator R&D in the Technical Design Phase* (2013), [arXiv:1306.6353 [physics.acc-ph]]. <https://doi.org/10.48550/arXiv.1306.6353>
- [17] P. A. Coe et al., *Meas. Sci. Technol.* **15** 2175-2187 (2004). 10.1088/0957-0233/15/11/001
- [18] T. Behnke et al., *The International Linear Collider Technical Design Report - Volume 4: Detectors* (2013). <https://doi.org/10.48550/arXiv.1306.6329>